Comprehensive characterization of the irradiation effects of glassy carbon ☆

J. David Arregui-Mena [a,*], Takaaki Koyanagi [a], David A. Cullen [b], Michael J. Zachman [b], Yan-Ru Lin [a], Philip D. Edmondson [a,c], Yutai Katoh [a]

[a] Materials Science and Technology Division, Oak Ridge National Laboratory, 1 Bethel Valley Road, Oak Ridge, TN 37830, USA
[b] Center for Nanophase Materials Science, Oak Ridge National Laboratory, 1 Bethel Valley Road, Oak Ridge, TN 37830, USA
[c] Department of Materials, The University of Manchester, Oxford Road, United Kingdom of Great Britain and Northern Ireland, Manchester M13 9PL, UK

Abstract

Carbon materials have become increasingly diverse, finding applications in high-temperature and high-radiation environments. Glassy carbon, an allotrope known for its exceptional chemical inertness and desirable mechanical properties. However, understanding neutron irradiation effects in glassy carbon has proven challenging, primarily because of its unique nanopore structure. This study presents a highly detailed microstructural characterization investigation of neutron-induced changes in glassy carbon, revealing how changes in nanopore structure and crystallinity impact the irradiation-induced shrinkage. Aberration-corrected scanning transmission electron microscopy (STEM) reveals pore closure that leads to material densification in the irradiated samples. Dimensional analysis combined with comparison to historical data suggest significant length shrinkage to occur. Neutron and in situ electron irradiation experiments suggest that glassy carbon transforms into so-called carbon onions, supporting the concept of shrinkage saturation. Investigating irradiation temperature effects using STEM, electron energy loss spectroscopy, x-ray diffraction, and Raman spectroscopy revealed partial amorphization at 210°C–230°C and preserved order in glassy carbon at 860°C, coinciding with pore closure. Thermal property measurements were also conducted to assess the effects of densification and other changes in the atomic structure of glassy carbon. The results of this study have broad implications in the deployment of glassy carbon to nuclear environments, based around the observed changes in the thermal properties, and demonstrates the operational window for the onset of densification.

* Corresponding author. E-mail: arreguimenjd@ornl.gov (J. David Arregui-Mena)

1 Introduction and Background

Glassy carbon is part of a group of monoatomic carbon materials capable of forming various allotropes via hybridizations of covalent bonds (sp, sp^2, or sp^3) [1]. Some differences between glassy carbon and other common carbon allotropes are its short-range crystalline order, a significant presence of defects, and its unique nanopore structure. Although glassy carbon can be classified as a structurally amorphous material, it cannot be compared to amorphous carbon such as activated carbon, carbon black, or carbon dots due to the presence of planar 2D structures formed by sp^2 bonds that are normally not present in amorphous carbons. Other carbon allotropes to glassy carbon formed by sp^2 hybridized aromatic carbon are graphite and certain varieties of pyrolytic carbons. Depending on the raw materials and manufacturing conditions, the overall stability of pyrolytic carbons and graphite can be improved by using thermal treatments. However, traditional methods cannot fully graphitize glassy carbon because of its relative stability at temperatures close to 3200°C [2]. Graphitization of glassy carbon can be achieved under high-stress conditions at high temperatures [3] or by combining high pressure and temperature treatments [4, 5].

Furthermore, graphite's porosity is more easy to observe than in glassy carbon because it is usually present at multiple length scales [6]. By contrast, glassy carbon exhibits a more well-defined size distribution of pores in the range of a few angstroms to several nanometers [7]. Another fundamental difference between glassy carbon and nongraphitizable materials is the possible presence of cross-linking of carbon domains [8]. Cross-linking is believed to be a feature of glassy carbon that refers to carbon atoms that form bridges between well-aligned carbon fragments.

Glassy carbon's impermeability to gas molecules [9] and potentially to molten salts [10, 11] have made it an attractive material for molten salt reactor (MSR) applications and fusion reactors that employ molten salts [12]. In particular, glassy carbon has been applied as a coating on nuclear graphite components to reduce the contact and impregnation of molten salts into nuclear graphite components [10, 11]. Moreover, glassy carbon was once considered for use in the first wall of

fusion reactors [13] and to contain radioactive waste [14]. Nowadays, carbon-based or carbon-focused materials are no longer deemed promising for fusion applications [15].

Glassy carbon can potentially be used as a coating material or to infiltrate the pores of nuclear graphite for molten reactor designs. In some instances, glassy carbon has been combined with other materials, such as pyrocarbon, to further improve the permeability and protection of MSR graphite components from molten salts [10] by applying a coating on the surface. Some publications [16-18] suggest that the sealant material used to infiltrate the pores of CGB graphite used in the molten salt reactor experiment was impregnated with furfuryl alcohol polymer, which is a common precursor of glassy carbon. Thus, glassy carbon or a similar material might already be used as a sealant material in MSR applications.

Several researchers have shown that neutron irradiation has a less significant effect on the mechanical properties of glassy carbon than nuclear graphite. Perhaps the earliest research paper on neutron irradiated glassy carbon was prepared by Shimada and Kikuchi [19]. This study investigated the effects of neutron irradiation on the electrical resistivity of heat-treated glassy carbon specimens. Shimada and Kikuchi [20] continued these studies by performing thermal resistivity, Young's modulus, and additional electrical resistivity measurements in thermally treated neutron-irradiated glassy carbon. This research shows that glassy carbon properties only decrease by a few tenths of the original values under neutron irradiation of 1.15×10^{20} n/cm^2 and over temperatures that range from 150°C to 200°C. Another example of neutron-irradiated glassy carbon experiments was published by Gray et al. [21]. Their efforts focused on analyzing dimensional changes and estimating the crystallite size of thermally treated specimens irradiated at a temperature of 550°C–650°C and fluence of 1.64×10^{21} n/cm^2 (E > 0.18 MeV). This research provides valuable evidence that the processing temperature can improve glassy carbon irradiation stability (less shrinkage). An irradiation campaign by Maruyama and Harayama [13] compared the effects of neutron irradiation in two graphite grades (IG-110U and ETP-10), a carbon–carbon composite (CX-202U), and glassy carbon (GC-30). The glassy carbon and two grades of graphite specimens were exposed to a lower irradiation temperature of 200°C and fluences of 1.38×10^{19} to 1.92×10^{20} n/cm^2 (E > 1 MeV). Under these irradiation conditions, the glassy carbon shrunk, whereas the graphite grades expanded. More recently, the combined efforts of Virgil'ev and

Lebedev [22] characterized multiple mechanical properties of glassy carbon, including dimensional change, weight, density, electric resistivity, dynamic Young's modulus, coefficient of thermal expansion, microhardness, and bending strength. A follow-up manuscript by Lebedev et al. [23] describes the mechanical property values of specimens exposed to other irradiation conditions. Although all this research provides a general understanding of the behavior of glassy carbon under irradiation, it does not characterize the microstructure that determines the underlying mechanisms that promote the changes.

This manuscript aims to bridge that knowledge gap by describing the possible mechanisms that control the dimensional change and thermophysical properties of glassy carbon at different irradiation temperatures. This research employed a novel and unique multiscale approach that combined aberration-corrected scanning transmission electron microscopy (STEM), energy loss spectroscopy (EELS), x-ray diffraction (XRD), and Raman spectroscopy. Three irradiation temperatures were used in this research to contrast the different responses of glassy carbon to neutron irradiation. Lower irradiation temperatures were used to promote the amorphization of the carbon domains and change the material's overall pore structure. Higher irradiation temperatures were used to investigate how neutron irradiation influence the mobility and densification of the bulk and graphite-like domains. To complement the microstructural analysis, the application of previously published theories describes the densification and atomic structure mechanisms that change glassy carbon's thermal diffusivity and specific heat capacity. The results obtained in this research were compared with other carbon-based materials used in the nuclear industry such as graphite and a carbon–carbon composite. Comparisons between these materials can aid in the elucidation of the effects of neutron irradiation in sp^2 allotropes of carbon. Furthermore, this research helps evaluate the possible applications and viability of glassy carbon in the nuclear industry and improves the understanding of irradiation effects and dimensional stability of some phases of nuclear graphite, pyrocarbons, and the carbon interface in SiC/SiC composites.

2 Materials and Methods

Typical properties of the glassy carbon specimens provided by the vendor are summarized in Fig. 1. The optical and scanning electron microscopy micrographs included in Fig. 1 also show the

surface and shape of the specimens. Nine samples manufactured by Tokai Carbon (product ID: GC20SS) were irradiated at the High Flux Isotope Reactor (HFIR) at Oak Ridge National Laboratory (ORNL). The irradiation temperatures (210°C–860°C) and total neutron fluences (~2 × 10^{25} n/m^2, E > 0.1 MeV) are summarized in Fig. 2. The manufacturer did not provide the precursor or temperature used to process the material because of its proprietary and business-sensitive nature.

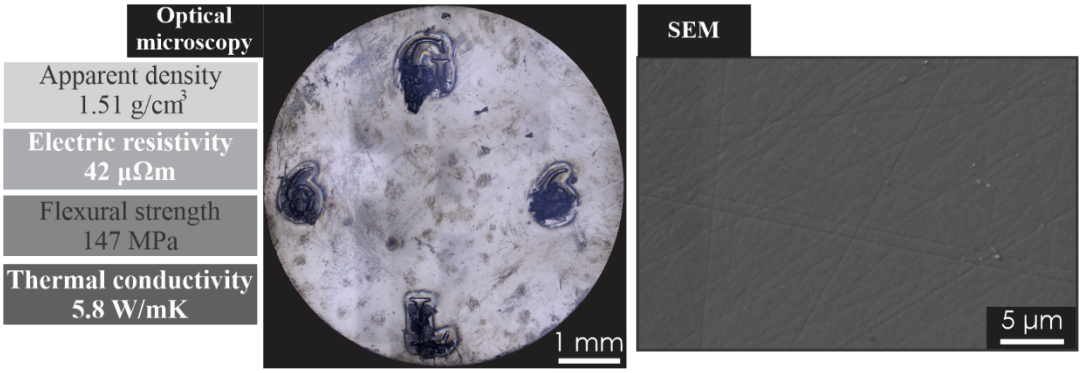

Figure 1. Stitched optical micrograph of a specimen and scanning electron micrographs of the surface of the glassy carbon samples with (inset) typical properties of Tokai Carbon's glassy carbon. The dark regions are the engravings used to identify each sample.

The specimens are nominally 6 mm in diameter and 0.5 mm thick. The irradiation temperatures were experimentally determined during annealing by tracking the recovery behavior of the instantaneous coefficient of thermal expansion of a passive thermometer made of high-purity chemical vapor deposited SiC using a NETZSCH DIL402CD horizontal dual pushrod dilatometer [24]. Typically, temperature can be accurately determined within about 15°C. A summary of the techniques, irradiation conditions, and measurements of the glassy carbon are provided in Fig. 2.

Unirradiated and neutron-irradiated samples of PCEA nuclear graphite and FMI-222 were used for comparison with the neutron-irradiation effects in glassy carbon. PCEA graphite is an extruded medium-fine grained graphite manufactured by Graftech [6]. The two PCEA samples were irradiated at 670°C and 900°C and neutron doses of 5.6 and 10.1 displacements per atom (dpa), respectively. Fiber Materials Incorporated manufactured the carbon–carbon composites (FMI-222). A P-55 pitch-based fiber and a mesophase pitch matrix form the FMI-222 specimens. Two

neutron-irradiated samples were used for the analysis, both irradiated at 500°C and 6 dpa. Additional information on the carbon–carbon composites is available in the literature [25].

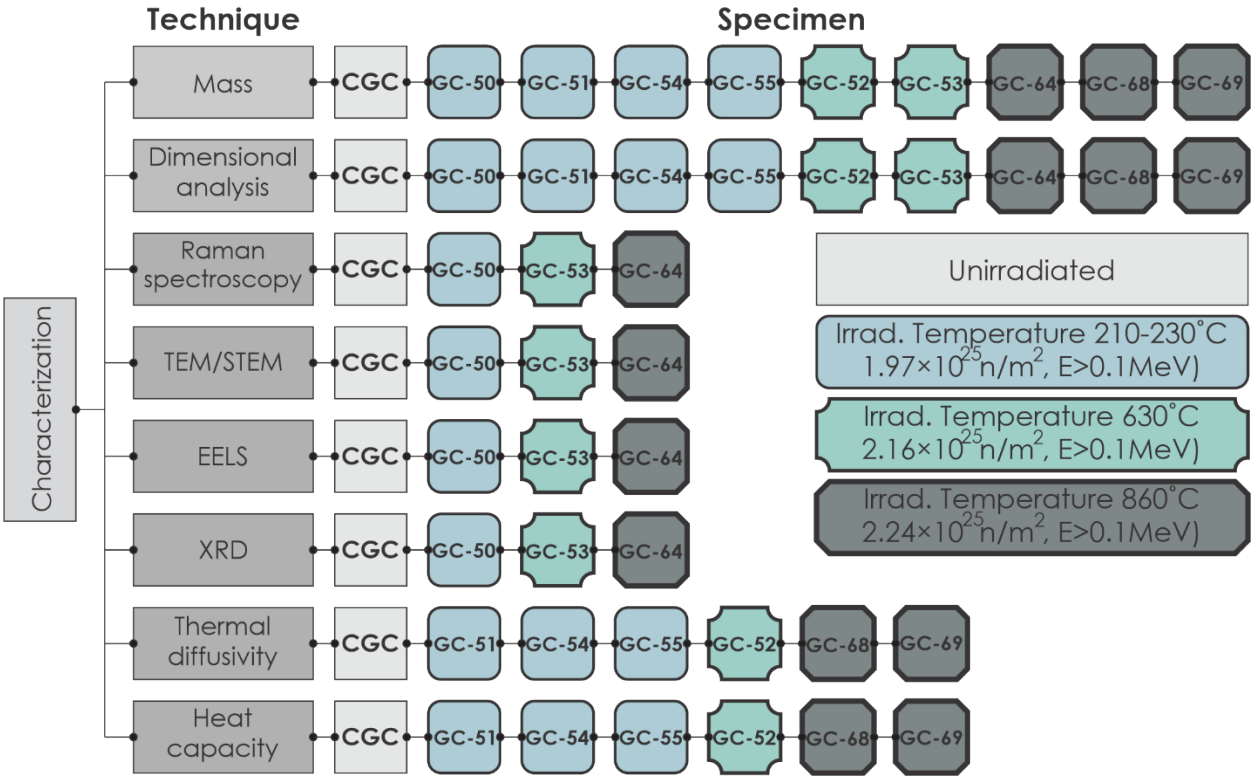

Fig. 2. Experimental matrix and irradiation conditions. CGC refers to control glassy carbon samples, GC refers to irradiated glassy carbon specimens.

2.1 Mass and Dimensional Measurements and Thermal Properties

The specimens' densities were determined according to ASTM C559-90 [26] and ASTM C38-96 [27]. These standards provide general guidance on estimating the bulk density of graphite and other carbon materials using mass and dimensional measurements. A mass balance and Vernier calipers were used for mass and dimensional analysis. The thermal conductivity of the specimens was determined from thermal diffusivity and specific heat capacity measurements. A Netzsch LFA467 apparatus measured thermal diffusivity, and a Netzsch DSC 404 measured specific heat capacity. The thermal conductivity of the specimens was estimated by using Eq. (1):

$$k = \alpha \rho C_p \#(1)$$

where α is the thermal diffusivity, k is the thermal conductivity, ρ is the specimen's density, and C_p is the measured specific heat capacity.

2.2 Raman Spectroscopy and X-Ray Diffraction

Raman spectroscopy experiments were performed in a Renishaw inVia confocal Raman microscope operated at a laser wavelength of 532 nm using a 2.5 mW laser power and an objective lens of ×50. Using a 532 nm laser, the probing depth penetration for graphite has been estimated to be around 50 nm, or about 150 graphite layers [28]. A total of 10 single-point spectra were taken from each selected sample surface. These spectra were averaged to represent each sample's spectrum. In addition, the same procedures and settings were used to acquire the spectrum of single-crystal silicon for reference and calibration. The spectrum range was taken from 0 and 3500 cm^{-1} to represent the D, G and D′ characteristic glassy carbon bands. It was assumed that no overlapping effect would come from the G and D′ bands. Each glassy carbon specimen measurement was probed at different locations to obtain a more representative bulk material Raman scattering signal. The average spectra were processed using WiRE 5.6 software.

XRD measurements were performed with a Panalytical X'Pert PRO XRD instrument. These measurements were acquired to complement the Raman spectroscopy and EELS measurements. A polymer film was placed on the stage of the XRD to protect the instrument from contamination and as a reference to confirm that the X-rays penetrated through the thickness of the sample. The polymer film had some degree of crystallinity that was subtracted from the spectra of the neutron-irradiated samples.

2.3 Transmission and Scanning Transmission Electron Microscopy and *In Situ* Electron Irradiation Experiments

Thin foils were prepared using focused ion beam milling; the specimen preparation methodology is described elsewhere [29]. The thin foils were further treated with a Fischione Model 1040 NanoMill. This instrument generates a low-energy argon ion beam to remove any residual ion amorphization or ion implantation during the initial sample preparation ensuring clean specimen surfaces. Liquid nitrogen cooling was used to reduce the temperature of the specimens

(approximately −165°C). A two-stage milling procedure was employed. First, the samples were milled at low incident angles of ±10° at an energy of 900 eV and emission current of 170 μA for 3 min. Then, the same procedure was followed at a lower energy of 600 eV for 2 min.

The prepared specimens were imaged via STEM and EELS using an aberration corrected JEOL NEOARM STEM operated at an accelerating voltage of 80 kV and equipped with a Gatan GIF965 Quantum ER spectrometer. Crystallite size spacing measurements of the short-order graphite-like structures were estimated directly from the STEM images and derived from the fast Fourier transform of five images at each condition.

Carbon K-edge (285 eV) spectra were acquired from the thin foils and were used to characterize the irradiation effects of the specimens in the as received and at the two irradiation conditions listed in Figure 2. To compare the glassy carbon samples, additional microstructural characterization was performed for PCEA nuclear graphite and FMI-222 specimens using a JEOL 2100F transmission electron microscope operated at an accelerating voltage of 80 kV in bright-field mode.

Two additional experiments were designed to elucidate the mobility of carbon strands under the presence of electron irradiation. In this case, the electron beam damage was used as a surrogate mechanism to simulate the mobility of the graphitic strands of glassy carbon and a chaotic structure found in a thin foil of PCEA nuclear graphite. A JEOL 2100F operated at an accelerating voltage of 200 kV was used for the *in situ* electron irradiation experiment. The electron irradiation was conducted at room temperature. An unirradiated glassy carbon specimen was sectioned from the bulk sample. This smaller portion of the sample was then crushed, diluted in an alcohol solution, and then mounted on a transmission electron microscopy (TEM) microgrid. This type of specimen preparation ensures the presence of thin areas of only a few stacks of graphitic planes. Electron dose calculations were estimated using the illuminated diameter at the image screen, current density readings, magnification, and time. The diameter of the electron beam was 50 mm on the viewing screen. This beam size allowed good imaging conditions and a current density of 25.1 pA/cm^2, which was high enough to induce changes in the thin areas of the glassy carbon particle. For the *in situ* electron irradiation experiment, the selected area of intestate was a large chaotic

structure formed by graphitic strands. In this case, the PCEA thin foil was irradiated continuously by the electron beam for 40 min. Bright-field TEM micrographs were captured every 10 min to document the evolution of the microstructure.

3 Results and Discussion

3.1 Dimensional Changes

Length changes of the irradiated samples acquired along with archival historical references are reported in Figure 3a. As shown in Figure 3a, the shrinkage of the specimens tends to be more acute in the samples exposed to higher neutron fluences. The plot in Figure 3a also highlights the effect of various degrees of crystallinity achieved by the processing temperatures employed during manufacturing. In the case of samples used by Gray et al. [21] and Lebedev et al. [23], different processing temperatures were used during manufacture. The samples used by Gray et al. experienced maximum processing temperatures of 1000°C (GC-10), 2000°C (GC-20), and 3000°C (GC-30); the Lebedev et al. specimens were processed at temperatures of 1300°C (SU-1300) and 2000°C (SU-2000). In the case of Gray et al. [21], the samples processed at a higher temperature had a better dimensional stability than the ones produced at lower temperatures. Similarly, the samples irradiated by Lebedev et al. [23] that were processed at a higher temperature experienced the least shrinkage. Specimens processed at higher temperatures during manufacture likely provide better dimensional stability under irradiation. TEM characterization of glassy carbon produced at different processing temperature conditions supports the idea that higher temperature processing might improve the material's local crystallinity [7].

Additional conclusions can be derived from the data points obtained in this study (Figure 3). The irradiation temperatures in the currently investigated specimens are lower or higher than the historical data points. In the case of the dimensional analysis on the modern specimens, the highest irradiation temperature caused more significant shrinkage than the lowest irradiation temperature. Temperatures close to 630°C appear to follow the same trend as the historical data. These results show the relationship between the type of defects and irradiation temperature in glassy carbon. The analysis of the other techniques will cover a more in-depth investigation of the defect formation.

Figure 3a results are also significant because they can be used to draw parallels between the mechanisms that drive the dimensional change of graphite and glassy carbon. Glassy carbon and graphite microstructures are related: both are allotropes of carbon formed by sp^2 hybridized aromatic rings. Figure 3a shows that, like nuclear graphite, glassy carbon shrinks under neutron irradiation. However, the dimensional change data for glassy carbon in Figure 3b does not follow the typical trend of a phenomenon known as turnaround in graphite. Turnaround would be the characteristic dose at which the material—in this case, glassy carbon—would reverse shrinkage and grow back to its original dimensions. By contrast, nuclear graphite undergoes more complex volumetric dimensional changes induced by neutron irradiation: the bulk material shrinks, then reaches a point at which the material starts to swell back to its original dimension, and then continues its growth until the differential crystal strain causes the eventual disintegration of the component [25]. Figure 3b was included to contrast the dimensional changes produced by neutron irradiation in glassy carbon and graphite G347A [30]. Like glassy carbon, nuclear graphite dimensional stability under irradiation is also dependent on processing temperatures. Higher graphitization temperatures have been shown to delay the turnaround effect in PGA nuclear graphite [31].

Neutron-induced bulk dimensional changes in graphite are attributed to defects introduced in the crystallites that modify its dimensions and crack closure [32]. However, no well-defined mechanism describes the shrinkage of glassy carbon. An essential difference between glassy carbon and nuclear graphite is the relatively low density of the material. Although the pores in glassy carbon cannot be observed in the bulk material (Figure 1), the density of glassy carbon (apparent density 1.58 g/cm^3 measured in this research) is lower than nuclear graphite (apparent density between 1.72 and 1.85 g/cm^3 [6]). The glassy carbon porosity and low density appear to accommodate the damage and swelling of the graphite-like parallel domains. The densification and eventual turnaround of glassy carbon may require even larger neutron doses, but these doses would have to be significantly higher than the doses at which turnaround is observed in standard nuclear graphite grades. Additional irradiation experiments to significantly higher doses—potentially much higher doses than are technologically relevant—would be required to conclude whether glassy carbon reaches a point at which turnaround can occur.

The comparison between dimensional changes of these two materials is also important because glassy carbon has been proposed as a coating material for graphite components in MSR designs [10]. As mentioned before, glassy carbon can be used as a sealant material or to partially infiltrate the porosity of graphite as in the CGB grade. Differential dimensional shrinkage/swelling under neutron irradiation might limit the applications of glassy carbon as a coating, especially at low neutron-irradiation doses, or may require temperature treatments to achieve better dimensional matching under neutron irradiation. In contrast, using glassy carbon in infiltration pores might be a viable alternative, as the Molten Salt Reactor Experiment demonstrated. CGB samples exposed to molten salts only gained 0.03% in weight after exposure to the reactor environment [33]. It is important to note that the infiltration of glassy carbon into CGB induced cracking and defects in some graphite components [34, 35]. However, alternative materials with similar properties could be produced without the presence of cracks [34]. The reactor designers did not replace the graphite components in CGB then because introducing new batches of graphite materials without defects would have caused a delay of at least a year in the MSRE experiments [36].

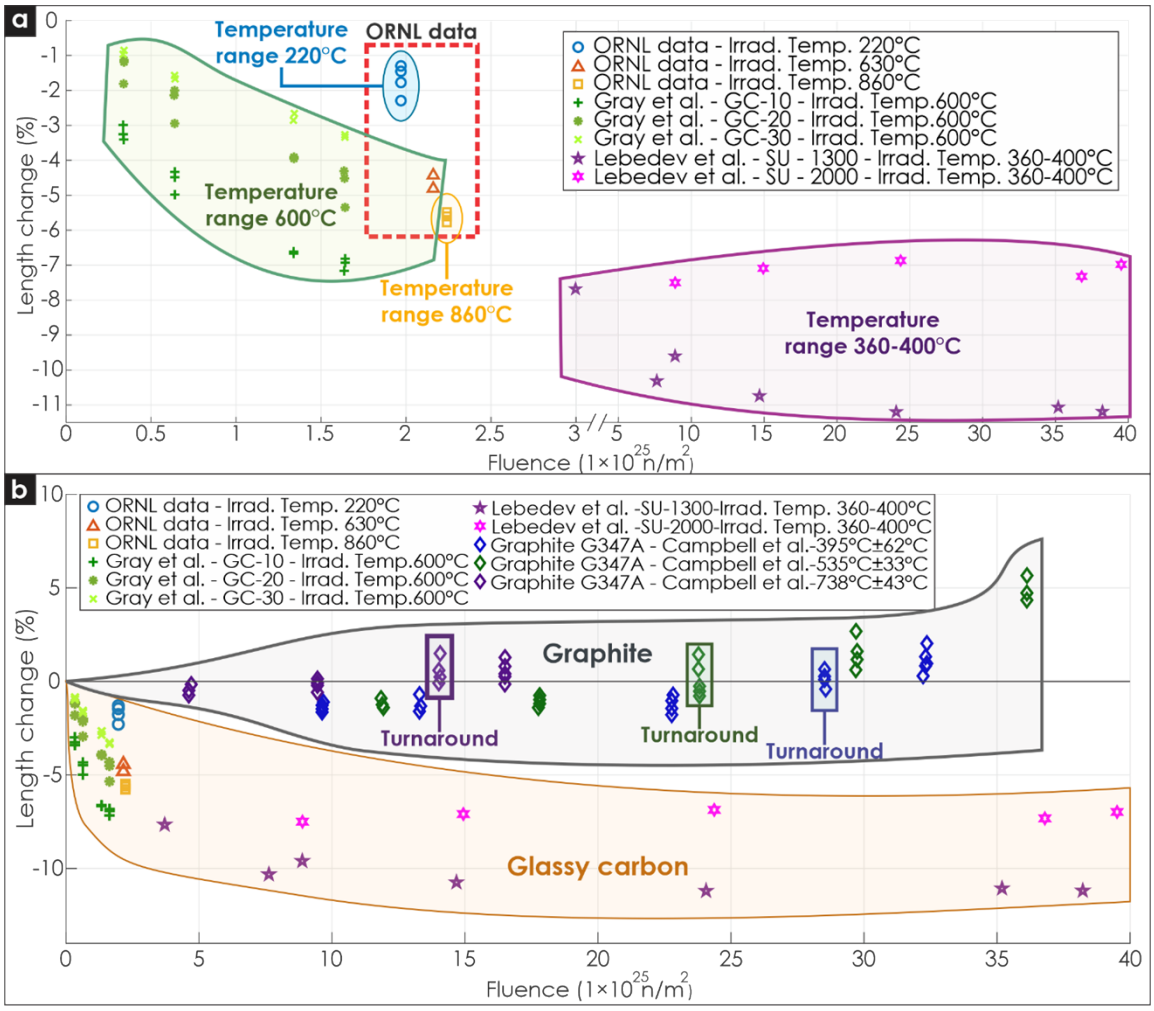

Figure 3. Neutron-induced length changes induced in glassy carbon samples and nuclear graphite grade G347A. (a) Data for glassy carbon obtained from this research and historical data. (b) Data for glassy carbon and nuclear graphite G347A in the axial direction [30]. The energy fluence by Gray et al. [21] and Lebedev et al. [23] are $E > 0.18$ MeV; the neutron energy of this manuscript is given at $E > 0.1$MeV.

3.2 Microstructural Changes Caused by Neutron Irradiation

To better understand the dimensional stability behavior and irradiation effects in glassy carbon, STEM imaging was performed along with EELS, Raman spectroscopy and XRD. Figure 4 shows aberration-corrected bright-field (BF)STEM micrographs of the glassy carbon obtained from the as-received material and the low and high irradiation temperature conditions. Aberration-corrected imaging enables better quality images and higher resolutions than conventional TEM imaging. When these micrographs are compared, it is possible to observe the closure of pores of glassy

carbon and the presence of different features before and after neutron irradiation. The control sample micrograph in Figure 4a displays the typical features of glassy carbon: the presence of nanopores as well as graphite-based structures with large curvatures. Nanopores are a common feature in glassy carbon [37] that can be easily observed throughout the control sample micrographs (Figure 4b), as is the curling and folding of the carbon domains (Figure 4a to Figure 4c). The presence of curved and bent graphite-like domains is correlated with the presence of non-six-membered rings [38]. Overlapping segments are also important recurring features in Figure 4a to Figure 4l. The overlap of segments might suggest crossovers between ordered graphite fragments. However, *In situ* TEM of the pyrolysis process suggests that the crossovers between domains might be a visual effect caused by the projections of two plains of two intersected domains [39].

Neutron irradiation changes the microstructure of glassy carbon (Figure 4a to Figure 4c) with respect to the original structure that contains gaps between graphitic domains. Changes in porosity can be observed at all irradiation conditions (Figure 4d and Figure 4l). The pore closure and shrinkage under irradiation appear to have two mechanisms, depending on the irradiation temperature. At low irradiation temperature (210°C), a significant structural change and pore closure appears to be driven by the disorder in the carbon strands (Figure 4d to Figure 4f). As shown in the high-magnification micrograph, most of the original linear features of the unirradiated specimen (Figure 4c) turn into highly curved and disordered strands (Figure 4f).

At the medium (630°C) and highest irradiation temperature (860°C), the closure of pores appears to be driven by a rearrangement of the graphitic-like strands rather than a loss of crystallinity (Figure 4g and Figure 4j). As can be seen from the bottom row of micrographs in Figure 4h and Figure 4k the graphite-like domains appear to coalesce, closing some of the pores and preserving the graphite-like strands. Another possible consequence of neutron irradiation at the medium and high temperatures is the changes of curvature of the graphite-like domains. The irradiation processes appear to promote the migration of graphitic fragments (Figure 4i and Figure 4l). Additional TEM data and analysis is provided in a complementary Data in Brief manuscript.

The interlayer separation or crystalline size of carbon atoms in Figure 4 for the control and high-temperature samples were directly measured to be approximately 3.5 Å. At the low irradiation temperature, the sample had too little short-order fragments for direct measurements to derive the crystalline size spacings. To further explore the spacing between ordered structures, radial averaged fast Fourier transform intensity profiles of five micrographs for each condition were employed to measure interlayer separation. The measurements show an increase in inter-layer separation for both irradiation conditions (3.7 Å) compared to the unirradiated specimen (3.5 Å), albeit within the instrument error margin. This apparent interlayer spacing increase partially explains the closure of pores shown in Figure 4f and Figure 4l. The lattice distances measured in this research are within the range of measurements published elsewhere [39] and are close to the interlayer separation of graphite (3.35 Å).

After irradiation, the graphite-like strands appear to preserve some of the original defects found in the unirradiated material (Figure 4c) that cause misalignments in the basal planes and limit a large-order graphitic stacking. Figure 4h suggests that the rearrangement of graphitic fragments can occasionally form fully closed structures or fullerenes (Figure 4h). This type of reorganization in carbon domains has also been called carbon onions. Carbon onions can be produced by different procedures, including electron beam irradiation [40, 41], mechanical milling [42, 43], chemical vapor deposition [44], and arc discharge [45], among other synthesis or phase-transformation methods. Carbon onions are formed through a self-organization process occurring in non-equilibrium conditions that can be facilitated under a form of irradiation [46]. A similar phenomenon has also been documented for neutron-irradiated quinoline-insoluble (QI) particles or chaotic regions in a phase of nuclear graphite [47-49]. A QI particle's cross section looks like a rosette structure formed by graphitic strands surrounded by a solid shell of graphitic planes. The graphitic carbon strands observed inside QI particles are very similar to the domains that form glassy carbon. In the presence of neutron irradiation, the rosette structures inside the QI particles evolve into solid round spheres formed by concentric carbon atoms, creating an onion-like appearance. Evidence of the local phase transformation of glassy carbon into carbon onions is indicated by orange arrows in Figure 4k.

To simulate the formation of carbon onions in glassy carbon, an unirradiated sample was irradiated at room temperature with an electron beam operated at 200 kV for 7 min (Figure 5). Electron irradiation can mimic some of the conditions of high-temperature treatment or neutron irradiation. Thermal treatments and, in some cases, electron irradiation can facilitate the structural fluidity in which the carbon atoms can restructure [41]. Examples of some of the first *in situ* electron irradiation experiments were are for carbon black [50] and carbon soot [41]. The series of images in Figure 5 shows the densification and rearrangement of the carbon atoms into several onion-like structures. These micrographs show that glassy carbon can be locally transformed into carbon onions, possibly inducing densification. Initially, the carbon domains are deformed and curved. After exposure to the electron beam, the carbon atoms start to rearrange, as shown in the micrographs in Figure 5. A closer inspection of the high-magnification micrograph of the high-temperature irradiated specimen in Figure 4 shows that some regions contain overlapped, round, closed structures that might be transitioning into carbon onions or fully closed fullerenes. It is important to mention that most of the carbon onions or structures generated by electron beam irradiation are not stable when the material is irradiated at room temperature. Carbon onions generated at room-temperature and electron irradiation are highly defective and formed by dissentious planes. Over time, the onions will decay and turn back into some form of disordered carbon, as shown by [51, 52].

Figure 5 also might explain the continuous densification mechanisms that glassy carbon undergoes at higher neutron doses at temperatures above 500°C. Glassy carbon might not recover its original dimensions under neutron irradiation (Figure 3). Research on the behavior of pyrolytic magnetic carbons [53] has shown that graphite-like fragments can contain large fractions of edge radicals that continuously attempt to achieve thermodynamically stable arrangements. Most of these graphitic fragments appear to have highly reactive edges [41]. Under irradiation, these fragments appear to favor the creation of round and closed fullerene structures or onion-like structures. During this process, the carbon onions might keep recombining or splitting into smaller spheres. The division or separation of carbon spheres is known to happen when carbon soot particles are exposed to electron irradiation [41]. Microstructural characterization of glassy carbon specimens exposed to higher neutron doses is needed to understand and confirm why glassy carbon appears not to undergo turnaround as nuclear graphite does.

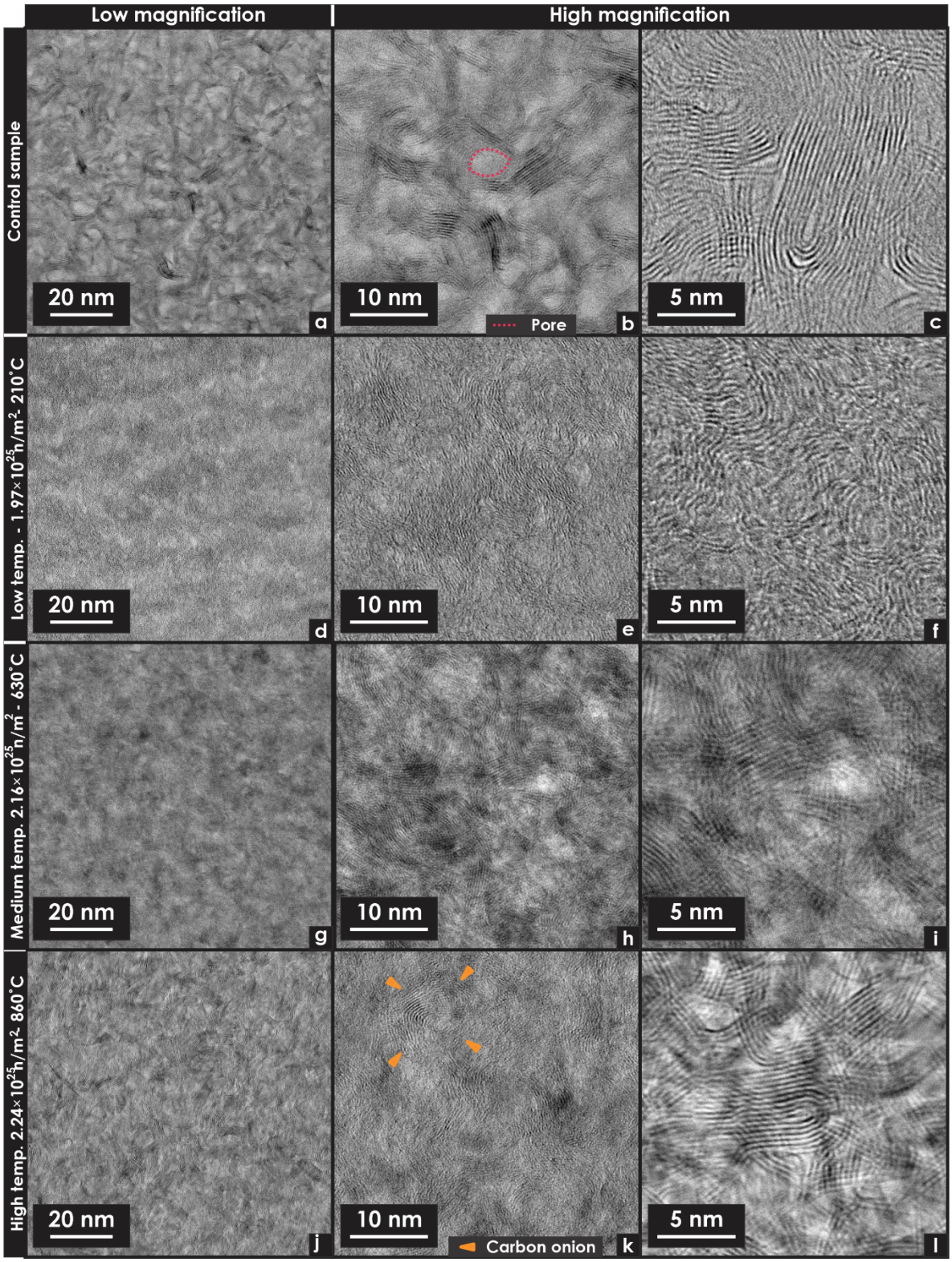

Figure 4. Aberration-corrected BF-STEM micrographs of as-received and neutron-irradiated glassy carbon specimens. The dotted line corresponds to pores in the original microstructure, and orange arrows highlight circular regions similar to carbon onions.

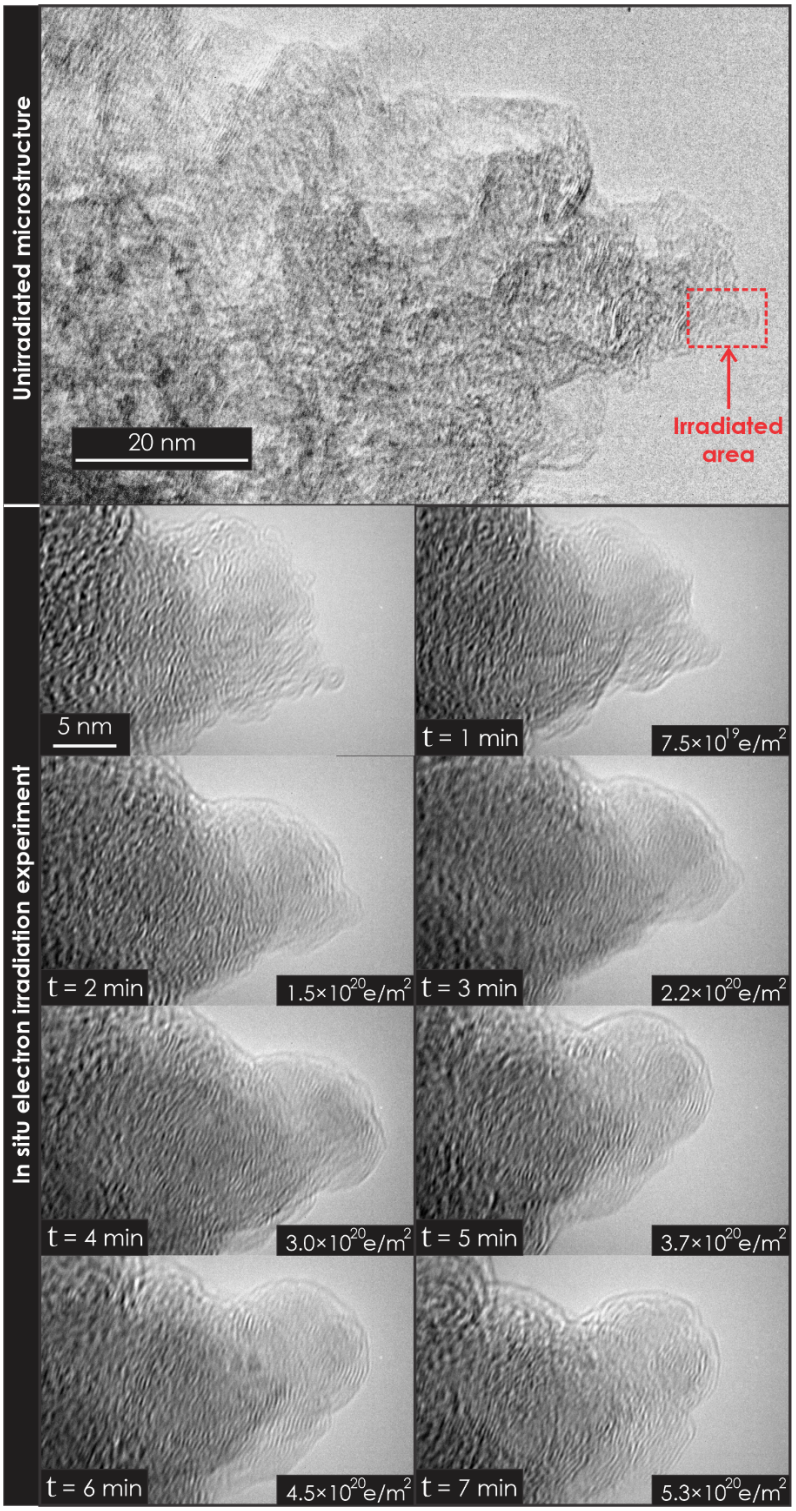

Figure 5. *In situ* electron irradiation experiment in a particle of glassy carbon. Bright-field TEM micrographs. These micrographs demonstrate the high mobility of carbon under the presence of the electron beam. The time of the experiment is shown in the lower left corners, and electron dose is shown in the lower right corners.

A thin foil of PCEA graphite was also irradiated similarly to the glassy carbon specimen. This experiment was conducted to show that some non-graphitizable inclusions of nuclear graphite can behave as glassy carbon. For this purpose, a chaotic region that contained large randomly oriented graphitic strands was selected for the experiment (Figure 6a). This region of the PCEA foil contained graphitic strands similar to the carbon structures found in glassy carbon. Under the electron beam, the graphitic strands' random positioning starts to transition to form onion-like structures at the center of the chaotic structure (Figure 6b to Figure 6e). At the end of the experiment (Figure 6e), several onion-like structures were created around the center of the chaotic structure (Figure 6f). Although graphite is subjected to graphitization, some non-graphitizable material tends to behave as glassy carbon under electron irradiation. Comparing Figure 5 and Figure 6 suggests that disordered graphitic content can behave similarly to glassy carbon under electron irradiation. More importantly, these results – using electron beam irradiation as a proxy for neutron irradiations – indicate that a fraction of nuclear graphite might behave as glassy carbon, shrinking at a different rate than highly graphitic material. Research on electron and neutron irradiation effects in nuclear graphite has also shown the generation of highly curved structures and incompletely closed fullerene-like defects in graphite [54, 55]. These morphological changes suggest that some defects generated in the graphite lattice might promote the non-six-membered rings and highly reactive edges found across the short-order carbon fragments in glassy carbon (Figure 4c, Figure 4i, Figure 4l).

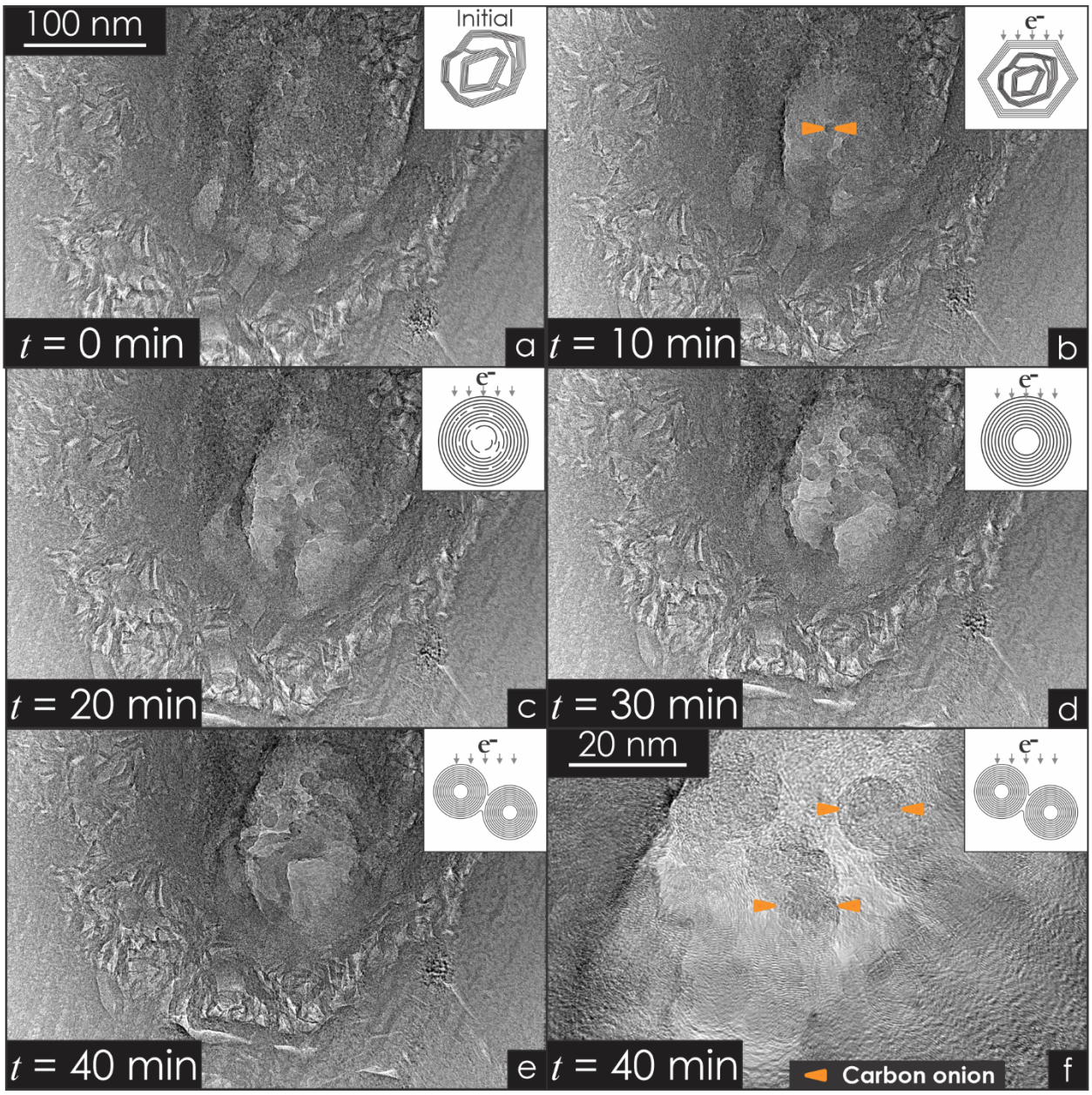

Figure 6. *In situ* electron irradiation experiment in chaotic region of graphite PCEA. Bright-field TEM micrographs were collected over 40 min. The irradiation time is shown in the lower left corners. The top right diagrams show the original and evolution of the original microstructure as a function of electron dose. The initial disordered, ribbon-like structure evolves into onions across the center of this chaotic structure. The orange arrows highlight the initial formation of carbon onions and the location of two large carbon onions.

To complement the imaging portion of this research, EELS, Raman spectroscopy, and XRD measurements were taken from the same samples characterized in Figure 4. First, the top of Figure 7a shows the EELS spectra of the as-received material and two irradiated samples. The energy range of the EELS spectrum includes the two characteristic peaks, the π* edge close to 285 eV, the broader σ* edge at 290 eV, and a plateau in between the two peaks. The π* peak is often related to the presence of sp^2 bonding and arises because of excitations of the 1s core level electrons to the anti-bonding π* state. The σ* peak is caused by the transitions of the carbon atom 1s core level electrons to the antibonding σ state. As shown in Figure 7a, the low irradiation temperature caused significant loss of intensity of both π* and σ* peaks compared with the as-received and high irradiation temperature samples. By contrast, the EELS spectra at the highest irradiation temperature remain similar to the as-received material. These results support the previous result about the microstructural changes based on the results Figure 4. Low irradiation temperatures induce amorphization in glassy carbon, whereas the higher irradiation temperature retains the local order in the carbon strands.

Raman spectroscopy results of the unirradiated and irradiated specimens are shown in Figure 7b. The most important peaks and respective motions for graphitic materials are indicated in Figure 7b. First, the peak that represents the disorder in the crystalline structure at 1350 cm^{-1}, also known as D peak, and the peak that represents the graphite-like structures, or G peak, for glassy carbon found around 1590 cm^{-1}. The G mode of graphite can be interpreted as the bond-stretching motions of pairs of carbon sp^2 atoms. This mode does not necessarily require the presence of sixfold rings and may be produced by other formations of sp^2 sites. By contrast, the D peak is a breathing mode that is not present in perfect graphite materials.

The Raman spectra in Figure 7b indicate that the lowest temperature irradiation induced amorphization of the specimens, as confirmed previously by the STEM and EELS results. For this irradiation condition, peaks D and G both became broader, and the overall spectra became similar to the ones found in amorphous carbon films [56]. The broadening and merging of D and G peaks can be observed in more disordered carbon materials. At lower irradiation temperatures, the nanopores in the pristine microstructure of glassy carbon (Figure 4) were filled by the amorphized

graphitic strands. Similarly, a study on the irradiation effects of ions in glassy carbon that included Raman spectroscopy has linked the amorphization with this material's eventual densification [57].

By contrast, the combined effect of irradiation and temperatures above 630°C increased the intensity values of the G peak (Figure 7b). No significant changes in the positions of the peaks were found at higher irradiation temperatures. However, the G peak also became broader under these conditions. An increment on the G peak does not necessarily mean that irradiation-induced crystallization occurred. Pioneering research [21] on the effects of irradiation-induced changes in glassy carbon crystallinity showed a decrease of order in crystallite size at an irradiation temperature of 600°C. Nevertheless, other research has shown that neutron irradiation increased crystallite size in pyrocarbons [58, 59]. These results show that neutron irradiation and high temperatures produce a synergistic effect that modifies the initial structure of glassy carbon that might generate a larger Raman intensity value of the G peak.

To complement and confirm the previous results, XRD measurements were conducted. X-rays penetrate deeper into the material, reducing the bias of localized measurements. Raman spectroscopy would have a penetration depth of about 50 nm in graphitic materials [28], whereas the XRD measurements can probe larger distances through the thickness of the specimen. The most significant change in the XRD results is in the diffractogram irradiated at the lowest irradiation temperature (Figure 7c blue diffractogram). No significant changes were observed in the diffractograms that belong to the other irradiation conditions or as-received material. Conventional XRD could resolve the partial amorphization of the low temperature irradiation specimen but not the changes in the other irradiated specimens.

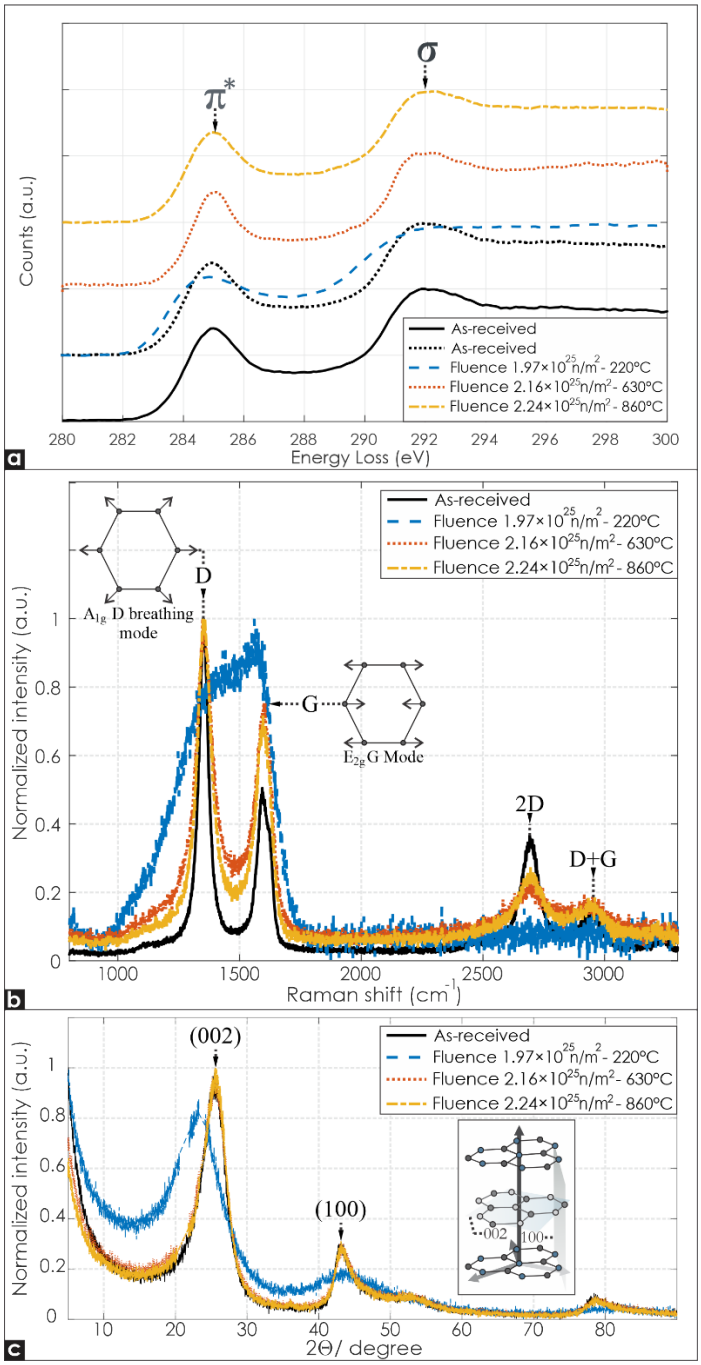

Figure 7. EELS, Raman spectroscopy, and XRD measurements for glassy carbon. (a) EELS spectra of as-received samples irradiated at low, medium and high temperatures. The as-received material (dashed lined) was included to contrast the difference between the original material and neutron irradiated specimen at low temperatures. (b) Normalized average Raman spectra of as-received and neutron-irradiated glassy carbon. (c) Normalized XRD diffractograms for as-received and neutron-irradiated samples.

3.3 The Effects of Neutron Irradiation on Thermal Properties

Figure 8a shows the specific heat capacity of the same specimens obtained at 100°C. Thermal diffusivity was measured at 20°C, 50°C, and 100°C; these values are plotted in Figure 8b. The thermal conductivity of the specimens at 100°C was derived from the thermal diffusivity and specific heat capacity measurements by using Eq. (1). These measurements were performed at these low temperatures to avoid annealing the irradiation damage and to minimize the release of Wigner energy of the low-temperature specimens.

In general, the heat capacity in carbon-based materials depends on the level of graphitization. Higher levels of graphitization lead to lower values of heat capacity, as have been showed by experimental methods [60-62]. Greater levels of amorphization lead to higher variations in bond strengths [63]. Increased levels of disordered in the specimens irradiated at the lowest temperature (Figure 4) explain the change in heat capacity after irradiation. In all cases, the irradiated specimens' heat capacity increased with respect to the as-received material (Figure 8a). The highest heat capacity values correspond to the lowest irradiation temperatures. Overall, the heat capacity of specimens irradiated at temperatures higher than 600°C experienced a less significant change than at the lowest irradiation temperature in the range of 210-230°C. Higher levels of disordered post-irradiation at the lowest temperature (Figure 4) explain the change in heat capacity values.

In Figure 8b, the differences in thermal diffusivity owing to neutron irradiation temperature are apparent. The lower the irradiation temperature, the lower the thermal diffusivity (Figure 8b) and thermal conductivity (Figure 8c). The most significant decrease in thermal diffusivity and conductivity corresponds to the lowest irradiation temperature conditions (blue lines). The changes in thermal diffusivity and thermal conductivity at the lowest irradiation temperatures could be linked to the loss of local crystallinity in the carbon strands. In graphitic materials, neutron-induced defects act as phonon-scattering locations that diminish the phonon mean free path and thus reduce the thermal conductivity [64].

The medium-dose and -temperature (orange line) glassy carbon specimen experienced a decrease in thermal conductivity of approximately 20% with respect to the unirradiated specimen.

At the medium temperature and dose, the thermal diffusivity reduction was more pronounced (33.6%) compared with the as-received material. By contrast, at the highest irradiation temperature and dose (yellow lines), the glassy carbon specimens retained most of their original thermal conductivity, but thermal diffusivity decreased. Densification and higher irradiation temperatures mitigate some of the effects of neutron damage or phase transformation at the highest dose. As with other graphitic materials, the rate of thermal conductivity reduction is a function of the creation and annealing of lattice defects and is therefore related to the irradiation temperature conditions. An extensive discussion of the links between irradiation temperature and thermal conductivity degradation is extensively described elsewhere [65].

Glassy carbon and graphitic materials exhibit a crucial distinction in their thermal conductivity. Materials such as pyrolytic graphites or vapor-grown carbon fiber have high thermal conductivities on the order of 2200 W/mK at room temperature [66]. Thermal conductivity values of modern graphite grades are 116 W/mK for IG-110 [67] or 156 W/mK for G347A [30], two orders of magnitude above the values reported in Figure 7c. Glassy carbon's poor thermal conductivity reflects the lack of long-range-order crystallinity compared with graphitic materials. This study is significant in part because the thermal properties of the glassy carbon specimens irradiated at low temperatures might be used to estimate the performance of carbon materials irradiated at low irradiation temperatures (<300°C). This assumption might be valid because irradiation at low temperatures favors the amorphization of carbon materials, which share a similar microstructure with the glassy carbon specimens irradiated at low temperatures. Moreover, the neutron-induced microstructural changes observed at medium and high irradiation temperatures (pore closure and changes in the curvature of coherent domains) can partly explain the variations of thermal properties with respect to the control sample (Figure 8). The changes in densification and microstructural changes also impact other mechanical properties, as shown in other studies[20, 22, 23].

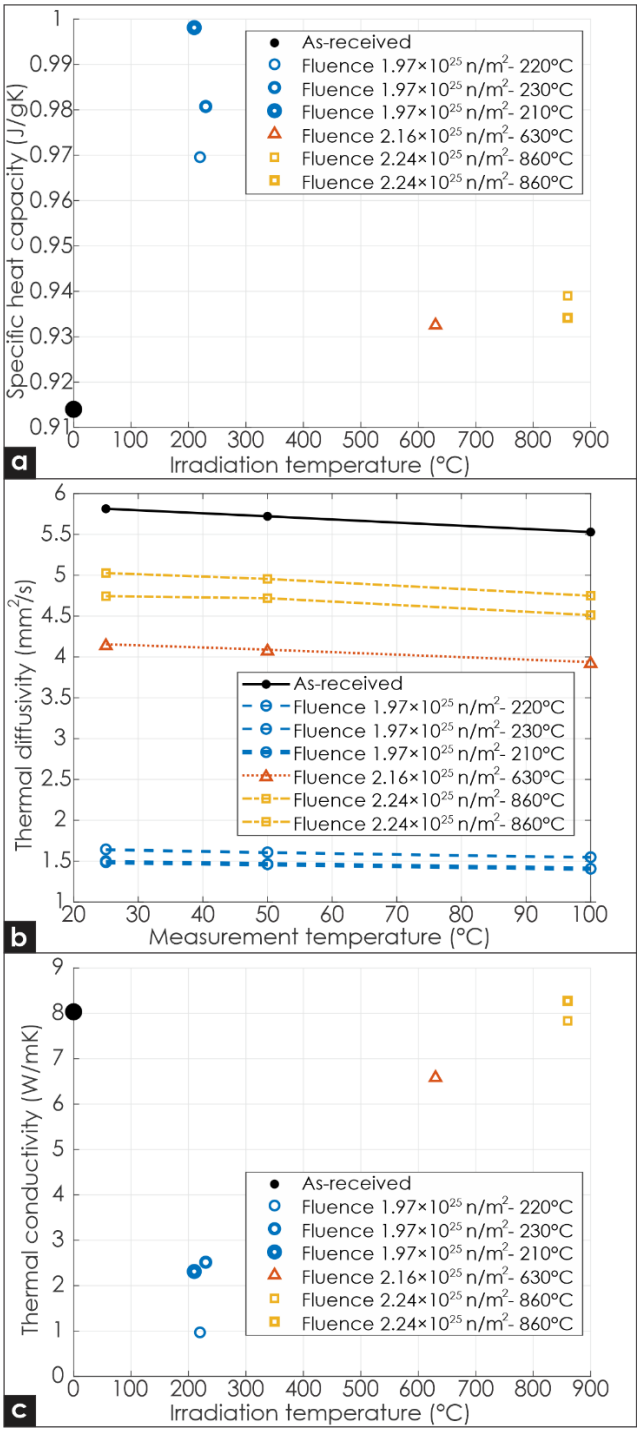

Figure 8. Thermal diffusivity, specific heat capacity, and thermal conductivity of as-received and neutron-irradiated specimens. (a) Specific heat capacity of as-received and low, medium, and high irradiation temperature samples estimated at 100°C. (b) Thermal diffusivity of as-received and low, medium, and high irradiation temperature samples. (c) Thermal conductivity of as-received and low, medium, and high irradiation temperature samples estimated at 100°C.

3.4 Comparison of Glassy Carbon Neutron Irradiation Effects with Carbon Fibers and Neutron Graphite

This section compares the irradiation effects of glassy carbon with two other prospective materials for fission nuclear applications: (1) a carbon fiber used in FMI-222 carbon–carbon composite and (2) PCEA nuclear graphite. Figure 9 shows the unirradiated and neutron-irradiated specimens of the three materials. The top row (Figure 9a to Figure 9c) shows the unirradiated microstructure of the materials. The first (Figure 9a) and second (Figure 9b) top micrographs illustrate the similarities between the unirradiated microstructure of glassy carbon and some particular locations inside this type of carbon fiber. Both materials are formed by the curly-folded graphite-like strands (Figure 9a and Figure 9b). By contrast, nuclear graphite can contain highly long-range-ordered graphitic material, and some regions contain poorly graphitized regions, such as the QI particles marked by red arrows in Figure 9c. Micrographs taken from the neutron-irradiated carbon fiber (Figure 9e and Figure 9h) and nuclear graphite show the presence of fullerene-like defects (Figure 9f and Figure 9i). Both types of defects are similar to the large folded curved structures found in the as-received and neutron-irradiated glassy carbon specimens (Figure 9a and Figure 9g).

The respective micrographs of the neutron-irradiated carbon fiber (Figure 9f-Figure 9i) and PCEA nuclear graphite show some of the first evidence of possible neutron-induced glassification. In this case, the glassification of the materials could be understood from the introduction of defects in the graphite lattice that turns into short-range bent and fully closed fullerene structures. Neutron irradiation might create non-six-membered rings that generate the bent and curved structures commonly found in glassy carbon.

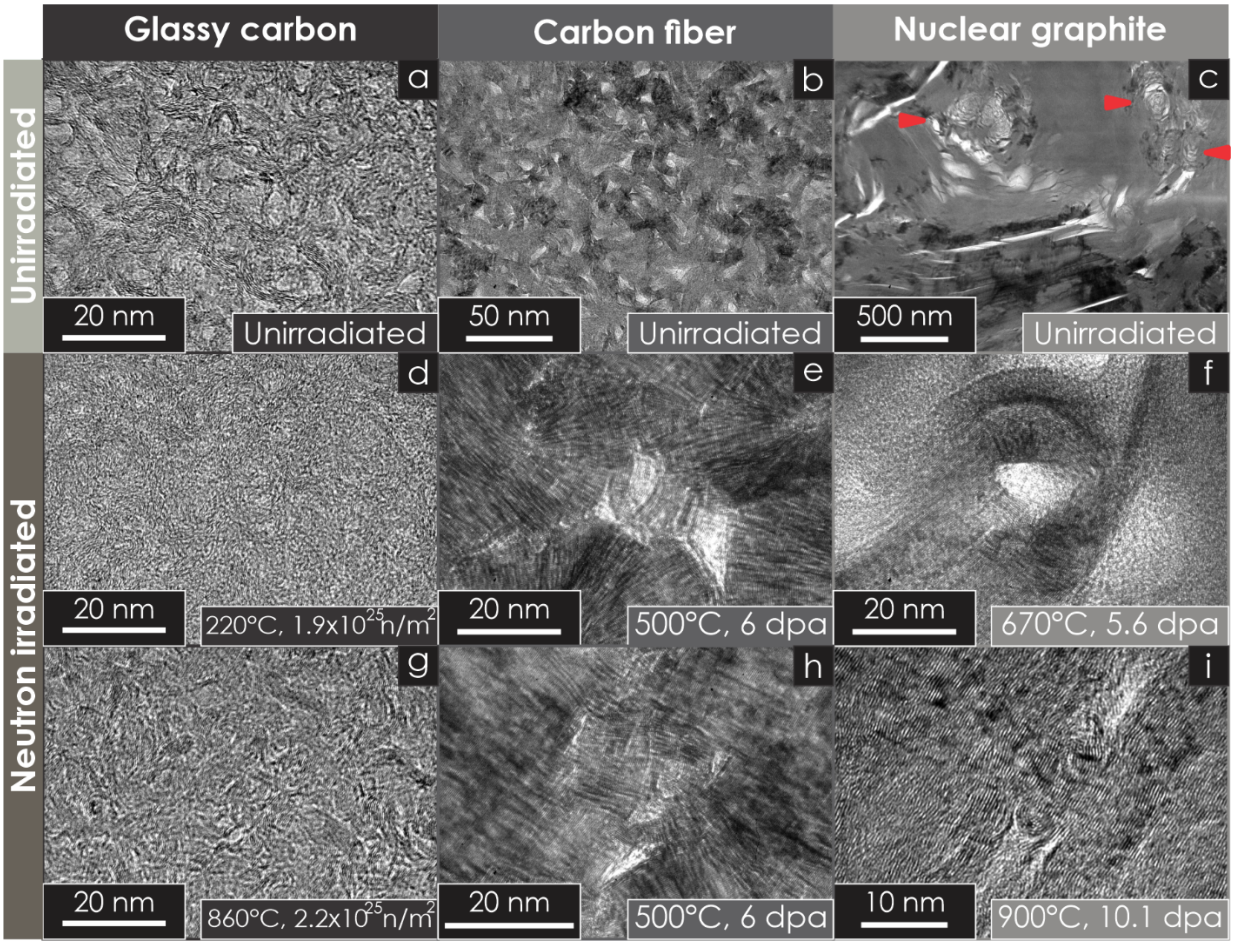

Figure 9. Bright-field TEM micrographs of as-received and neutron-irradiated specimens of glassy carbon, carbon fiber, and PCEA nuclear graphite. This compendium of images shows the typical unirradiated microstructures of these materials and some of their defects generated by neutron irradiation.

4 Conclusions

This research bridges the knowledge gap regarding how neutron irradiation affects the crystal and nanopore structure in glassy carbon by elucidating the potential mechanisms that govern dimensional changes and thermophysical properties of glassy carbon at varying irradiation temperatures. This study identified the following conclusions:

a) Neutron irradiation leads to the shrinkage of glassy carbon. Irradiation temperature is one of the most critical factors contributing to this dimensional change. Data points collected by other authors (Figure 3) suggest that the initial crystallinity of the material can delay the

shrinkage of the material. Higher processing temperatures produce more dimensionally stable materials under the effects of neutron irradiation.

b) Glassy carbon's dimensional change might not have a turnaround point like graphitic materials. The phase transformation from glassy carbon into carbon onions along with the rearrangements of short-order structures appear to be contributing factors that stop the swelling of the material. Short-order structures can be found across carbon fibers and nuclear graphite. The partial fullerenization of curve sections within carbon composites and nuclear graphite might translate into having the same dimensional change as glassy carbon.

c) Neutron-induced shrinkage appears to be a function of pore closure. At the lowest irradiation temperatures, decreased pore size was produced by the partial amorphization of carbon strands (Figure 4). For the higher irradiation temperatures, the pores appear to close because of the partial phase transformation into carbon onions and an increase in interlayer spacing.

d) *In situ* electron irradiation demonstrates the possible transformation of glassy carbon into carbon onions (Figure 5). Repeating the electron irradiation experiment in a chaotic structure found in a PCEA specimen demonstrated that this transformation can also be found in some regions of nuclear graphite.

e) The partial amorphization of the specimens irradiated at the lowest temperature range (210°C to 230°C) was confirmed by using STEM, EELS, Raman spectroscopy, and XRD (Figure 6). The highly defective structure of the glassy carbon (Figure 4f) demonstrated a reduction of the short-order structures in this material.

f) Despite the lack of long-range crystalline order in glassy carbon compared with highly graphitic materials, these materials have similar relationships between irradiation temperature and thermal conductivity changes. As in graphitic materials, lower irradiation temperatures led to a larger decrease in thermal conductivity.

g) Although glassy carbon is a non-graphitizable material, it bears some relation to some phases contained in carbon composites and non-graphitizable material contained in nuclear graphite. The neutron-irradiated specimens of PCEA graphite and carbon fiber show that some regions can glassify. In other words, some regions can transform into highly curved

regions or fully closed fullerenes. These defects indicate the presence of non-six-member rings commonly found in glassy carbon.

The crystallinity levels produced by neutron irradiation at temperatures above 630°C remain unclear. Additional evidence is required to confirm the phase transformation of glassy carbon into carbon onions under neutron irradiation. In the future, electron tomography characterization [68] will be conducted to better understand the closure and initial nature of the porosity in glassy carbon.

Acknowledgements

A portion of this work was supported by the US Department of Energy (DOE) Office of Nuclear Energy under DOE Idaho Operations Office Contract DE-AC07- 051D14517 as part of a Nuclear Science User Facilities experiment, "Microstructural characterization of neutron irradiated C–C composites" (23-1908). A portion of this research used the resources of the Low Activation Materials Development and Analysis Laboratory, a DOE Office of Science research facility operated by the Oak Ridge National Laboratory (ORNL). Neutron irradiation was supported by the DOE Office of Fusion Energy Sciences under contract DE-AC05-00OR22725 and by IMR Tohoku University under contract NFE-13-04416 with UT-Battelle, LLC. The post-irradiation examination was also partially supported by the DOE Office of Fusion Energy Sciences, Fusion Materials Program. A portion of this research used resources at the High Flux Isotope Reactor, a DOE Office of Science User Facility operated by ORNL. STEM and EELS research was supported by ORNL's Center for Nanophase Materials Sciences, which is a DOE Office of Science user facility. The authors acknowledge ORNL's Materials and Chemistry Group in the Nuclear Nonproliferation Division for use of the Raman spectrometer. The authors also acknowledge Shawn S. Reeves for her assistance with sample preparation and Stephanie M. Curlin for the thermal property measurements. The authors would like to thank Hughie Spinoza for his valuable comments and discussion.

References

[1] V. Uskoković, A historical review of glassy carbon: Synthesis, structure, properties and applications, Carbon Trends 5 (2021) 100116.

[2] T. Yamaguchi, Galvanomagnetic properties of glassy carbon, Carbon 1(1) (1963) 47-50.
[3] K. Kamiya, M. Inagaki, Formation of highly oriented layers of graphite in glass-like carbon heat-treated under pressure, Carbon 19(1) (1981) 45-49.
[4] C.Q. Jin, X. Wang, Z.X. Liu, Y.L. Zhang, F.Y. Li, R.C. Yu, The unusual morphology, structure, and magnetic property evolution of glassy carbon upon high pressure treatment, Brazilian Journal of Physics 33 (2003).
[5] L.A. Pesin, Review Structure and properties of glass-like carbon, Journal of Materials Science 37(1) (2002) 1-28.
[6] J.D. Arregui-Mena, R.N. Worth, W. Bodel, B. März, W. Li, A.A. Campbell, E. Cakmak, N. Gallego, C. Contescu, P.D. Edmondson, Multiscale characterization and comparison of historical and modern nuclear graphite grades, Materials Characterization 190 (2022) 112047.
[7] K. Jurkiewicz, M. Pawlyta, D. Zygadło, D. Chrobak, S. Duber, R. Wrzalik, A. Ratuszna, A. Burian, Evolution of glassy carbon under heat treatment: correlation structure–mechanical properties, Journal of Materials Science 53(5) (2018) 3509-3523.
[8] R.E. Franklin, J.T. Randall, Crystallite growth in graphitizing and non-graphitizing carbons, Proceedings of the Royal Society of London. Series A. Mathematical and Physical Sciences 209(1097) (1951) 196-218.
[9] M.-C. Huang, H. Teng, Urea impregnation to enhance porosity development of carbons prepared from phenol–formaldehyde resins, Carbon 40(6) (2002) 955-958.
[10] V. Bernardet, S. Gomes, S. Delpeux, M. Dubois, K. Guérin, D. Avignant, G. Renaudin, L. Duclaux, Protection of nuclear graphite toward fluoride molten salt by glassy carbon deposit, Journal of Nuclear Materials 384(3) (2009) 292-302.
[11] Z. He, J. Song, P. Lian, D. Zhang, Z. Liu, Excluding molten fluoride salt from nuclear graphite by SiC/glassy carbon composite coating, Nuclear Engineering and Technology 51(5) (2019) 1390-1397.
[12] R. Boullon, J.-C. Jaboulay, J. Aubert, Molten salt breeding blanket: Investigations and proposals of pre-conceptual design options for testing in DEMO, Fusion Engineering and Design 171 (2021) 112707.
[13] T. Maruyama, M. Harayama, Neutron irradiation effect on the thermal conductivity and dimensional change of graphite materials, Journal of Nuclear Materials 195(1) (1992) 44-50.
[14] J.B. Malherbe, O.S. Odutemowo, E.G. Njoroge, D.F. Langa, T.T. Hlatshwayo, C.C. Theron, Ion bombardment of glassy carbon, Vacuum 149 (2018) 19-22.
[15] Y. Nobuta, Y. Hatano, M. Matsuyama, S. Abe, S. Akamaru, Y. Yamauchi, T. Hino, S. Suzuki, M. Akiba, Tritium retention properties of tungsten, graphite and co-deposited carbon film, Fusion Engineering and Design 89(7) (2014) 1516-1519.
[16] E.I.R. B., J.L. Rutherford, A.P. Malinauskas, Gas transport in MSRE moderator graphite. II. Effects of impregnation. III. Variation of flow properties ORNL, Oak Ridge, Teneessee, 1969.
[17] R.B.E. III, J.L. Rutherford, R.B. Perez, Recoil of Fission Products. II. In Heterogeneous Carbon Structures, Journal of Applied Physics 39(7) (1968) 3253-3267.
[18] J.D. Arregui-Mena, P.D. Edmondson, D. Cullen, S. Levine, C. Contescu, Y. Katoh, N. Gallego, Microstructural characterization of the CGB graphite grade from the molten salt reactor experiment, Journal of Nuclear Materials 582 (2023) 154421.
[19] T. Shimada, T. Kikuchi, Neutron Irradiation Effects of Electrical Properties in Glassy Carbon, Journal of the Physical Society of Japan 20(7) (1965) 1288-1289.
[20] T. Shimada, T. Kikuchi, Neutron irradiation effect in glassy carbon, Japan, 1974, p. 19.

[21] W.J. Gray, W.C. Morgan, J.H. Cox, E.M. Woodruff, Irradiation-induced length changes of glassy carbon, Carbon 10(2) (1972) 236-238.
[22] Y.S. Virgil'ev, I.G. Lebedev, Effect of Neutron Irradiation on Properties of Glassy Carbon, Inorganic Materials 38(7) (2002) 668-673.
[23] I.G. Lebedev, S.A. Vorob'ev, V.D. Shushakov, Y.S. Virgil'ev, Neutron Irradiation Induced Changes in the Structure and Properties of Glassy Carbon, Atomic Energy 92(5) (2002) 381-385.
[24] A.A. Campbell, W.D. Porter, Y. Katoh, L.L. Snead, Method for analyzing passive silicon carbide thermometry with a continuous dilatometer to determine irradiation temperature, Nuclear Instruments and Methods in Physics Research Section B: Beam Interactions with Materials and Atoms 370 (2016) 49-58.
[25] L.L. Snead, T.D. Burchell, Y. Katoh, Swelling of nuclear graphite and high quality carbon fiber composite under very high irradiation temperature, Journal of Nuclear Materials 381(1) (2008) 55-61.
[26] ASTM, ASTM C559-90 - Standard Test Method For Bulk Density By Physical Measurements Of Manufactured Carbon And Graphite Articles, 2005.
[27] ASTM, ASTM C559-16 - Standard Test Method For Bulk Density By Physical Measurements Of Manufactured Carbon And Graphite Articles, 2020.
[28] Z. Ni, Y. Wang, T. Yu, Z. Shen, Raman spectroscopy and imaging of graphene, Nano Research 1(4) (2008) 273-291.
[29] J.D. Arregui-Mena, R.N. Worth, W. Bodel, B. März, W. Li, A. Selby, A.A. Campbell, C. Contescu, P.D. Edmondson, N. Gallego, SEM and TEM data of nuclear graphite and glassy carbon microstructures, Data in Brief 46 (2023) 108808.
[30] A.A. Campbell, Y. Katoh, M.A. Snead, K. Takizawa, Property changes of G347A graphite due to neutron irradiation, Carbon 109 (2016) 860-873.
[31] J.E. Brocklehurst, B.T. Kelly, Analysis of the dimensional changes and structural changes in polycrystalline graphite under fast neutron irradiation, Carbon 31(1) (1993) 155-178.
[32] H.M. Freeman, A.N. Jones, M.B. Ward, F.S. Hage, N. Tzelepi, Q.M. Ramasse, A.J. Scott, R.M.D. Brydson, On the nature of cracks and voids in nuclear graphite, Carbon 103 (2016) 45-55.
[33] M.W. Rosenthal, R.B. Briggs, P.R. Kasten, Molten-salt reactor program semiannual progress report for period ending August 31, 1967, ORNL, Oak Ridge, Tennessee, 1967.
[34] H.E. McCoy, J.R. Weir, Materials development for molten-salt breeder reactors, ORNL, Oak Ridge, Tennessee, 1967.
[35] P.R. Kasten, E.S. Bettis, W.H. Cook, GRAPHITE BEHAVIOR AND ITS EFFECTS ON MSBR PERFORMANCE, Nucl. Eng. Design, 9: 157-95(Feb. 1969). (1969) Medium: X.
[36] R.B. Briggs, Molten-salt reactor program semiannual progress report for period ending July 31, 1964, ORNL, Oak Ridge, Tennessee, 1964.
[37] P. Serp, 7.13 - Carbon, in: J. Reedijk, K. Poeppelmeier (Eds.), Comprehensive Inorganic Chemistry II (Second Edition), Elsevier, Amsterdam, 2013, pp. 323-369.
[38] C.L. Burket, R. Rajagopalan, A.P. Marencic, K. Dronvajjala, H.C. Foley, Genesis of porosity in polyfurfuryl alcohol derived nanoporous carbon, Carbon 44(14) (2006) 2957-2963.
[39] S. Sharma, C.N. Shyam Kumar, J.G. Korvink, C. Kübel, Evolution of Glassy Carbon Microstructure: In Situ Transmission Electron Microscopy of the Pyrolysis Process, Scientific Reports 8(1) (2018) 16282.
[40] F. Banhart, T. Füller, P. Redlich, P.M. Ajayan, The formation, annealing and self-compression of carbon onions under electron irradiation, Chemical Physics Letters 269(3) (1997) 349-355.

[41] D. Ugarte, Curling and closure of graphitic networks under electron-beam irradiation, Nature 359(6397) (1992) 707-709.
[42] J.Y. Huang, H. Yasuda, H. Mori, Highly curved carbon nanostructures produced by ball-milling, Chemical Physics Letters 303(1) (1999) 130-134.
[43] X.H. Chen, H.S. Yang, G.T. Wu, M. Wang, F.M. Deng, X.B. Zhang, J.C. Peng, W.Z. Li, Generation of curved or closed-shell carbon nanostructures by ball-milling of graphite, Journal of Crystal Growth 218(1) (2000) 57-61.
[44] A.G. Nasibulin, A. Moisala, D.P. Brown, E.I. Kauppinen, Carbon nanotubes and onions from carbon monoxide using Ni(acac)2 and Cu(acac)2 as catalyst precursors, Carbon 41(14) (2003) 2711-2724.
[45] D. Ugarte, Morphology and structure of graphitic soot particles generated in arc-discharge C60 production, Chemical Physics Letters 198(6) (1992) 596-602.
[46] B. Florian, Irradiation effects in carbon nanostructures, Reports on Progress in Physics 62(8) (1999) 1181.
[47] J.D. Arregui-Mena, R.N. Worth, M.A. Tunes, P.D. Edmondson, Observations of crystal strains in filler and QI particles through TEM examination – Effect of processing and grain size, Materials & Design 204 (2021) 109673.
[48] C. Karthik, J. Kane, D.P. Butt, W.E. Windes, R. Ubic, Neutron irradiation induced microstructural changes in NBG-18 and IG-110 nuclear graphites, Carbon 86 (2015) 124-131.
[49] C.I. Contescu, J.D. Arregui-Mena, A.A. Campbell, P.D. Edmondson, N.C. Gallego, K. Takizawa, Y. Katoh, Development of mesopores in superfine grain graphite neutron-irradiated at high fluence, Carbon 141 (2019) 663-675.
[50] S. Iijima, Direct observation of the tetrahedral bonding in graphitized carbon black by high resolution electron microscopy, Journal of Crystal Growth 50(3) (1980) 675-683.
[51] G. Lulli, A. Parisini, G. Mattei, Influence of electron-beam parameters on the radiation-induced formation of graphitic onions, Ultramicroscopy 60(2) (1995) 187-194.
[52] M.S. Zwanger, F. Banhart, A. Seeger, Formation and decay of spherical concentric-shell carbon clusters, Journal of Crystal Growth 163(4) (1996) 445-454.
[53] S. Sharma, A.M. Rostas, L. Bordonali, N. MacKinnon, S. Weber, J.G. Korvink, Micro and nano patternable magnetic carbon, Journal of Applied Physics 120(23) (2016).
[54] S. Johns, T. Poulsen, J.J. Kane, W.E. Windes, R. Ubic, C. Karthik, Formation of carbon nanostructures in nuclear graphite under high-temperature in situ electron-irradiation, Carbon 143 (2019) 908-914.
[55] S. Johns, L. He, K. Bustillo, W.E. Windes, R. Ubic, C. Karthik, Fullerene-like defects in high-temperature neutron-irradiated nuclear graphite, Carbon 166 (2020) 113-122.
[56] P.K. Chu, L. Li, Characterization of amorphous and nanocrystalline carbon films, Materials Chemistry and Physics 96(2) (2006) 253-277.
[57] D.G. McCulloch, S. Prawer, A. Hoffman, Structural investigation of xenon-ion-beam-irradiated glassy carbon, Physical Review B 50(9) (1994) 5905-5917.
[58] J.C. Bokros, G.L. Guthrie, A.S. Schwartz, The influence of crystallite size on the dimensional changes induced in carbonaceous materials by high-temperature irradiation, Carbon 6(1) (1968) 55-63.
[59] J.C. Bokros, R.J. Price, Dimensional changes induced in pyrolytic carbon by high-temperature fast-neutron irradiation, Carbon 5(3) (1967) 301-312.
[60] W. Desorbo, G.E. Nichols, A calorimeter for the temperature region 1–20°K—The specific heat of some graphite specimens, Journal of Physics and Chemistry of Solids 6(4) (1958) 352-366.

[61] B.J.C. van der Hoeven, P.H. Keesom, Specific Heat of Various Graphites between 0.4 and 2.0\ifmmode^\circ\else\textdegree\fi{}K, Physical Review 130(4) (1963) 1318-1321.
[62] P. Delhaes, Y. Hishiyama, Specific heat of soft carbons between 0.6° and 4.2° K—I, Carbon 8(1) (1970) 31-38.
[63] Y. Takahashi, E.F. Westrum, Glassy Carbon low-temperature thermodynamic properties, The Journal of Chemical Thermodynamics 2(6) (1970) 847-854.
[64] D.B. Timothy, Radiation damage in carbon–carbon composites: structure and property effects, Physica Scripta 1996(T64) (1996) 17.
[65] L.L. Snead, CHAPTER 12 - Fusion Energy Applications, in: T.D. Burchell (Ed.), Carbon Materials for Advanced Technologies, Elsevier Science Ltd, Oxford, 1999, pp. 389-427.
[66] R. Taylor, The thermal conductivity of pyrolytic graphite, The Philosophical Magazine: A Journal of Theoretical Experimental and Applied Physics 13(121) (1966) 157-166.
[67] B.J. Marsden, G.N. Hall, A.N. Jones, 4.13 - Graphite in Gas-Cooled Reactors☆, in: R.J.M. Konings, R.E. Stoller (Eds.), Comprehensive Nuclear Materials (Second Edition), Elsevier, Oxford, 2020, pp. 357-421.
[68] J.D. Arregui-Mena, D.A. Cullen, R.N. Worth, S.V. Venkatakrishnan, M.S.L. Jordan, M. Ward, C.M. Parish, N. Gallego, Y. Katoh, P.D. Edmondson, N. Tzelepi, Electron tomography of unirradiated and irradiated nuclear graphite, Journal of Nuclear Materials 545 (2021) 152649.